International Journal of Pharmaceutics 374 (2009) 153–161

Contents lists available at ScienceDirect

International Journal of Pharmaceutics

journal homepage: www.elsevier.com/locate/ijpharm

Pharmaceutical Nanotechnology

Mechanical stability of hollow spherical nano-aggregates as ultrasound contrast agent

Kunn Hadinoto*

School of Chemical and Biomedical Engineering, Nanyang Technological University, Singapore 637459, Singapore

ARTICLE INFO

Article history:
Received 9 December 2008
Received in revised form 9 March 2009
Accepted 11 March 2009
Available online 24 March 2009

Keywords:
Ultrasound contrast agent
Nanoparticles
Spray drying
Hollow particles

ABSTRACT

Gas-filled hollow nanoparticulate aggregates designed for use as an ultrasound contrast agent and as an ultrasound-mediated nanoparticulate drug delivery vehicle are manufactured by spray drying of nanoparticulate suspension at a fast convective drying rate. The gas outward diffusion from the hollow particles during insonication reduces the shell mechanical stability hence shortening the lifespan of the ultrasound contrast agent. The present work aims to develop a formulation method to produce micron-size hollow nanoparticulate aggregates with high shell mechanical stability by controlling the shell thickness-to-particle radius (S/R) ratio. The impacts of changing (1) the spray drying parameters, (2) nanoparticulate suspension concentration, and (3) surfactant inclusion (i.e. phospholipids) on the particle morphology and the S/R ratio are investigated. Biocompatible PMMA-MeOPEGMA nanoparticles of varying sizes (i.e. 50 ± 20, 110 ± 40, and 230 ± 80 nm) are used as the model nanoparticles. The results indicate that the S/R ratio increases with decreasing particle size and the shell mechanical stability is linearly dependent on the S/R ratio. The effects of the spray drying parameters and nanoparticle concentration are found to be minimal in the absence of the phospholipids. The S/R ratio can be significantly increased by using larger size nanoparticles with the phospholipids inclusion.

1. Introduction

Ultrasound imaging is one of the most widely performed non-intrusive medical diagnostic tests, whose operation relies on its ability to detect and quantify the backscattered acoustic signal from the organ tissue being imaged. The traditional ultrasound imaging, however, lacks the capability to image microvascular blood flow in an organ tissue due to the similar echogenicity levels of the backscattered acoustic signals from the tissue and the blood capillary. For that reason, hollow micron-size particles acting as an ultrasound contrast agent are locally delivered by an intravenous injection, prior to the tissue perfusion imaging, to enhance the signal amplitude of the blood flow relative to that of the tissue. Ultrasound contrast agents typically consist of a gas core that is encapsulated by a solid shell of polymer or lipid materials to form hollow gas-filled particles. In addition to their use as an ultrasound contrast agent, the hollow particles can also be employed as a targeted ultrasound-mediated drug delivery vehicle in which ultrasound-mediated destruction of the shell, which is loaded with the drug, triggers the therapeutic release (Chen et al., 2006; Lum et al., 2006).

The ultrasound contrast enhancement in the presence of the hollow particles is attributed to (1) a strong acoustic signal generated by the compressible gas, and (2) the large density difference between the gas-filled particles and the surrounding tissue (Lindner, 2004). The effectiveness of the ultrasound contrast agent is governed by (1) the particle size, (2) the gas aqueous diffusivity, and (3) the shell mechanical stability. A large particle size is preferred as it generates a strong acoustic signal. Nevertheless, the particle size must not exceed the blood capillary size (i.e. <10 μm) to ensure its capillary passage. To prolong the lifespan of the contrast agent, low diffusivity gases (e.g. perfluorocarbons) are often used in place of air to minimize the gas outward diffusion from the shell that is often defected during insonication.

The shell can be fragmented or even completely destructed under a strong ultrasound field allowing the gas to diffuse out through the shell defects. A polymeric shell is found to exhibit a higher mechanical stability than a lipid shell, though the lipid shell is easier to form via its self-assembly process and it exhibits a higher echogenicity level compared to the polymer shell (Ferrara et al., 2007). The shell mechanical stability of a hollow particle is governed in the classical mechanics theory by the ratio of the shell thickness to the particle radius (S/R), where S is the shell thickness and R is the hollow particle radius (Landau and Lifshitz, 1976). Hollow particles with a high S/R ratio are less prone to the fragmentation and consequently a higher ultrasound frequency is needed to destabilize the shell (Raisinghani and DeMaria, 2001).

* Tel.: +65 6514 8381; fax: +65 6794 7553.
E-mail address: kunnong@ntu.edu.sg.

0378-5173/$ – see front matter © 2009 Elsevier B.V. All rights reserved.
doi:10.1016/j.ijpharm.2009.03.017

Nevertheless, the use of a polymeric shell with an excessive S/R ratio has its drawbacks. First, the high S/R ratio indicates that a less amount of gas is being encapsulated resulting in a lower echogenicity level. Second, a rigid polymeric shell significantly increases the resonance frequency of the hollow particles, which necessitates the use of high-intensity ultrasound to achieve an optimal echogenicity level that is typically obtained at the resonance frequency of the ultrasound contrast agent (Goertz et al., 2007). The use of high-intensity ultrasound may negatively affect the polymeric shell integrity hence limiting the use of the hollow particles as a drug delivery vehicle (Rossi et al., 2008). Therefore, the ability to produce hollow particles with a controllable shell thickness is crucial in the design of ultrasound contrast agents.

A two-step process of emulsification followed by drying is typically employed to produce the hollow particles in the dry-powder form, which are later dispersed in an aqueous solution to create an injectable form of the ultrasound contrast agent. The process consists of (1) an emulsification step in which a liquid/solid core of a volatile foaming agent (e.g. ammonium bicarbonate) is encapsulated by a polymeric shell, and (2) a drying step in which the liquid/solid core is removed by either freeze or spray drying to create the hollow structure (Bjerknes et al., 1997; El-Sherif and Wheatley, 2003; Narayan and Wheatley, 1999; Straub et al., 2005). Alternatively, Pisani et al. (2006) describe a one-step emulsification technique to encapsulate liquid perfluorocarbons inside a polymeric shell to produce an aqueous suspension of microcapsules, whose S/R ratio is controlled by modifying the polymer-to-perfluorocarbons ratio. On a similar note, a production of nanocomposite hollow particles by homogenization of surfactant-coated polymeric nanoparticles using micron-size bubbles as a template is described by Schmidt and Roessling (2006).

In the present work, a novel yet simple technique to produce polymeric hollow particles with a controllable shell thickness, by means of spray drying of polymeric nanoparticulate suspension, is developed. The spray-dried particles exhibit a hollow structure, whose shells are composed of nanoparticulate aggregates that are held together by physical attractive forces (i.e. capillary and van der Waals forces). The simplicity of a spray drying process makes this technique significantly less time-intensive compared to the aforementioned techniques involving both emulsification and drying steps. Furthermore, the use of polymeric nanoparticles offers a versatile platform in ultrasound-mediated nanoparticulate drug delivery as the nanoparticles can be specifically formulated to suit the hydrophobicity and therapeutic release requirement of the drug.

The present technique was first developed by the authors to manufacture micron-size carrier particles of nanoparticulate drug for pulmonary drug delivery using a dry powder inhaler (Hadinoto et al., 2007). The specific aim of Hadinoto et al. (2007) was to manufacture hollow spherical nanoparticulate aggregates with a large geometric diameter ($d_G \approx 10$–$15\,\mu m$) to improve the aerosolization efficiency and therapeutic efficacy of the inhaled particles. The shell mechanical stability of the hollow nanoparticulate aggregates, however, was not examined by Hadinoto et al. (2007) because the particles were not to be exposed to high-intensity destabilizing forces in a dry powder inhaler. On the other hand, the shell mechanical stability is of significant importance in the present work as the hollow nanoparticulate aggregates are to be used as an ultrasound contrast agent that is routinely exposed to high-intensity ultrasonication.

The detailed physical mechanism behind the hollow nanoparticulate aggregate formation is illustrated in Fig. 1. Evaporation of the liquid from the droplet surface causes the nanoparticles at the receding liquid–vapour interface being exposed to the vapour phase. As the surface energy of a solid–vapour interface is greater than that of a liquid–vapour interface, the exposed nanoparticles migrate toward the droplet centre to minimize their surface energy. To produce the hollow nanoparticulate aggregates, a fast convective drying rate, where the time for the liquid evaporation is shorter than the time needed by the nanoparticles to diffuse back toward the droplet centre, is required. A fast convective drying rate is obtained when the local Peclet number (Pe) is significantly larger than unity. Pe defined in Eq. (1) signifies the relative importance of the time scale of the nanoparticle diffusion (R^2/D_S) with respect to that of the convective drying rate (τ_D).

$$Pe = \frac{r^2}{\tau_D D_S} \tag{1}$$

where r, τ_D, and D_S are the droplet radius, drying time, and nanoparticle diffusion coefficient, respectively.

For $Pe \gg 1$, the nanoparticle diffusion rate toward the droplet centre is slower than the convective drying rate hence resulting in the shell formation. As the shell begins to form, the capillary force generated by the meniscus formed in the gap between the nanoparticles drives the nanoparticles closer forming the nanoparticulate aggregates. This attractive capillary force, however, is resisted by the repulsive electrostatic force acting as a stabilizer against the aggregation process. The competing interaction between these two forces leads to a shell buckling phenomenon, which influences the resultant shell thickness and is manifested in the formation of dimpled spherical hollow particles (Tsapis et al., 2005).

Fig. 1 displays the three types of particle morphology that are typically formed due to the shell buckling phenomenon. They are (A) dimpled spherical hollow nanoparticulate aggregates with geometric diameter between 5 and 15 μm, (B) 2–5 μm convex-shaped solid (i.e. non-hollow) aggregates, and (C) very fine crumpled solid aggregates (<2 μm). The ideal morphology for the ultrasound contrast agent is the type A morphology with a controllable S/R ratio and geometric size smaller than 10 μm. The types B and C morphology are likely caused by (1) an excessive shell buckling that breaks the hollow nanoparticulate aggregates into non-hollow fragments, or (2) the presence of a surfactant that reduces the spray droplets stability causing their initially spherical shape to be easily distorted as the droplets travel along the drying chamber.

The specific aim of the present work is to develop a formulation method to produce hollow spherical nanoparticulate aggregates with controllable shell thickness and to examine the impact of varying shell thickness on the shell mechanical stability. For that purpose, the effects of (1) the spray drying operating condition, (2) the nanoparticulate suspension concentration, and (3) the surfactant inclusion (i.e. phospholipids) on the S/R ratio and particle morphology are investigated for a wide range of nanoparticle sizes. Biocompatible PMMA-MeOPEGMA nanoparticles (i.e. poly(methyl-methacrylate) conjugated with methoxy(polyethylene-glycol)methacrylate) are used as the model nanoparticle because acrylic-based polymer, such as PMMA-MeOPEGMA, is well known to exhibit a high mechanical strength suited for the spray drying process, where a high shear force is exerted by the drying gas on the spray droplets containing the polymeric nanoparticles.

2. Materials and methods

2.1. Materials

The monomers for the synthesis of the polymeric nanoparticles i.e. methyl methacrylate (MMA), butyl acrylate (BA), the initiator 4,4-azobis(4-cyanovaleric acid) (carboxy ADIB, purity ≥75%), ethanol, and ethyl acetate are purchased from Sigma–Aldrich. The methoxy(polyethylene glycol)methacrylate (MeOPEGMA, MW = 2000) is kindly supplied by Cognis Performance Chemicals (UK). Phospholipids S100 (95% phosphatidyl-

choline from fat free soybean lecithin) is obtained from Lipoid GmbH (Germany).

2.2. Preparation of PMMA-MeOPEGMA nanoparticles

The PMMA-MeOPEGMA polymer is prepared by a solution polymerization of MeOPEGMA, MMA, and BA in the proportions 15/74/11 (% w/w). Ethyl acetate and ethanol are used as the solvents. The polymer is converted into nanoparticles by the solvent replacement technique. The nanoparticles exhibit steric colloidal stability arising from the MeOPEGMA component. Briefly, 0.15 g carboxy ADIB is dissolved in 15 mL ethanol and 55 mL ethyl acetate is added. The solution is refluxed for 45 min at 90 °C in a water-cooled reflux condenser. For the 1st feed solution, 0.13 g carboxy ADIB and 12.7 g MeOPEGMA are dissolved in 6 mL ethanol. For the 2nd feed solution, MMA and BA monomers are mixed according to their weight fraction in a beaker. The volumes of both the feed solutions are made up to 50 mL by adding ethanol. The two feed solutions are added drop-wise into the refluxed solution, and the polymerization is run for about 2 h at 90 °C. At the end of the polymerization, the temperature is maintained at 90 °C to partially evaporate the ethyl acetate, while 50–100 mL ethanol is continuously added to prevent the polymer from drying out.

Next, the solvent is displaced by adding water drop-wise at 70 °C inducing a macromolecular rearrangement of the polymer to form colloidally stable nanoparticles. The nanoparticulate suspension is continuously heated at 70 °C to evaporate the remaining ethanol. Lastly, the nanoparticulate suspension is dialyzed for 24 h to remove excess monomers and solvents. A wide range of nanoparticle sizes are obtained by varying the amount of ethanol added after the polymerization step. The size and zeta potential of the nanoparticles is measured by dynamic light scattering using Zetasizer Nano-ZS (Malvern, UK). Suspensions of PMMA-MeOPEGMA nanoparticles (4% w/v) having mean diameters of 50 ± 20, 110 ± 40, and 230 ± 80 nm and zeta potential between +30 and 50 mV are obtained as a result. For the experiments involving the phospholipids, the spray drying suspension is prepared by dissolving the desired amount of phospholipids in 10 mL ethanol, which is next mixed with 90 mL ultrapure water containing the nanoparticles.

2.3. Spray drying experiment

Büchi B-290 Mini Spray Dryer (Switzerland), which operates on the principal of a two-fluid atomizer, is employed in the experiment. The nozzle diameter used is 1.5 mm. The adjustable parameters in the experiments are the inlet temperature, the drying gas flow rate, and the feed flow rate. The following spray drying condition is employed unless stated otherwise: inlet temperature of 110 °C, drying gas flow rate of 250 L/h, and feed rate of 4.0 mL/min. In the present work, compressed air is used as the drying gas; however, the technique allows air to be replaced by low diffusivity gases supplied at an elevated temperature. At the current inlet temperature, the spray dryer outlet temperature varies between 65 and 70 °C, which is slightly above the glass transition temperature of the PMMA-MeOPEGMA polymer (T_g = 65 °C) determined by a differential scanning calorimetry (PerkinElmer, USA). The calculated drying time (τ_D) of a single 50 μm droplet at 100 °C is ≈0.15 s, whereas the diffusion coefficient of 100 nm nanoparticles (D_S) is $\approx 10^{-12}$ m^2/s resulting in *Pe* of ≈1000 (Eq. (1)). Hence, the fast convective drying rate required to form the hollow nanoparticulate aggregates is satisfied at the current operating condition.

After spray drying, the dry powders are dispersed in ultrapure water by a gentle mixing to create an injectable form of the hollow nanoparticulate aggregates. In our preliminary study, the hollow particle suspension is ultrasonicated at a low intensity (40 kHz) for 5 min and next centrifuged at 8000 rpm at an ambient temperature. The resultant supernatant is analyzed using the Zetasizer to detect the presence of dispersed nanoparticles, if any. The Zetasizer analysis does not result in a significant difference between the particle size distribution of the fresh ultrapure water, which is con-

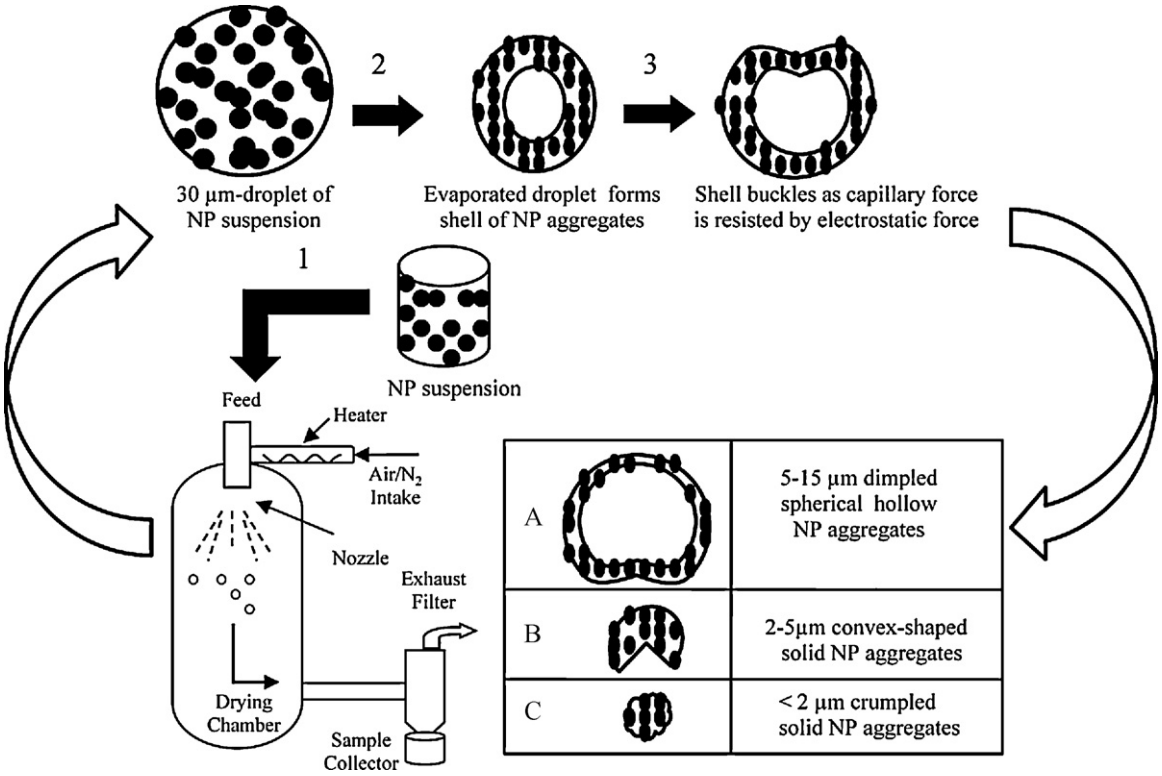

Fig. 1. The formation of hollow spherical nanoparticulate aggregates by spray drying.

tributed by the particulate impurities in the water, and that of the supernatant. The result therefore indicates that the nanoparticulate aggregates are not easily disintegrated into the primary nanoparticles in an aqueous environment. The shell mechanical stability of the hollow particles is being investigated under a high-intensity ultrasound. The results of the ultrasound attenuation as a function of frequency at different time intervals will be detailed in a forthcoming article.

2.4. Shell thickness characterization

The hollow nanoparticulate aggregates are characterized in terms of their size, size distribution, shape, and shell thickness. The spray-dried particles are stored in a desiccator for a 48-hour-period prior to the characterization. The particle geometric diameter (d_G) is determined by light diffraction using Particle Size Analyzer MS2000 (Malvern, UK). The results reported are based on measurements of three aliquots with a minimum of 1000 sample counts each. The measurement uncertainty for the d_G measurement is approximately 5%. The particle shape information is obtained using a Scanning Electron Microscope (SEM) model JSM-6700F (JEOL, USA). Transmission Electron Microscope (TEM) model Tecnai-TF-20 (FEI Company, USA) is used to examine the degree of hollowness of the particles. The samples for the SEM analysis are prepared by wetting the SEM carbon tape prior to sprinkling the particles onto them. The samples for the TEM analysis are prepared by re-suspending the spray-dried particles in ultrapure water after which 1 mL of the suspension is deposited on a copper grid covered with a formwar film (400 mesh) using a pipette. Both the SEM and TEM samples are dried in a desiccator prior to the analysis.

The ratio of the shell thickness to the particle radius in Eq. (2) is quantified using the degree of hollowness that is characterized by the ratio of ρ_{eff}/ρ_{true}, where ρ_{eff} and ρ_{true} are the effective and true particle densities, respectively. The derivation of Eq. (2) is provided in Appendix A. The effective particle density is defined as the particle mass divided by its total volume that includes the volume of the solid, hollow core, and pores, whereas the true particle density is calculated only based on its solid volume.

$$\frac{S}{R} = 1 - \left(1 - \frac{\rho_{eff}}{\rho_{true}}\right)^{1/3} \tag{2}$$

The ratio of ρ_{eff}/ρ_{true} is typically determined from direct measurements of the particle densities, where ρ_{true} and ρ_{eff} are determined by pcynometer (Ultrapcynometer1000) and tap densitometer (Autotap1000) of Quantachromme (USA), respectively. The value of ρ_{eff} obtained from the tap densitometer, however, is not only influenced by the degree of hollowness of the particles, but also by the interparticle surface forces. As a result, the tap density measurement is often inadequately sensitive to capture a small change in the degree of hollowness for particles with significant interparticle attractive forces (e.g. fine cohesive particles). In the present work, the size of the hollow nanoparticulate aggregates must be less than 10 μm to be suitable as an ultrasound contrast agent, hence significant interparticle forces exist. For that reason, the present work proposes an alternative method to quantify ρ_{eff} using the particle aerodynamic diameter data.

In inhaled drug delivery research, the particle aerodynamic diameter (d_A) can be related to ρ_{eff} by the geometric diameter (d_G) as described in Eq. (3) in which $\rho_S = 1\ \mathrm{g/cm^3}$ (Edwards and Dunbar, 2002). The aerodynamic diameter is defined as the diameter of a unit density spherical particle that settles through the air with a velocity equal to that of the particle in question. d_A is typically used to characterize the distance travelled by the inhaled particle in the human respiratory airways and is obtained using the time-of-flight measurement technique (PSDA 3603, TSI, USA). The results reported are based on three aliquots of 1000 sample counts each. The measurement uncertainty between the three replicates is less than 2%.

$$\rho_{eff} = \rho_S \left(\frac{d_A}{d_G}\right)^2 \tag{3}$$

Taking into account the measurement uncertainties of both d_G and d_A (i.e. 5% and 2%, respectively), the experimental uncertainty in the ratio of ρ_{eff}/ρ_{true} determined by Eq. (3) is as follows:

$$\frac{\Delta\rho_{eff}}{\rho_{eff}} = 2\left(\frac{\Delta d_G}{d_G}\right) + 2\left(\frac{\Delta d_A}{d_A}\right) \approx 14\% \tag{4}$$

2.5. Shell mechanical stability quantification

The shell mechanical stability is quantified using a mechanistic model of Krasovitski and Kimmel (2006), who studied the impact of the gas outward diffusion on the shell stability of a shrinking bubble. The model takes into account the inherent shell property (i.e. Young's modulus), the S/R ratio, and the surface tension to derive a critical particle radius (R_{crit}) at which the shell loses its mechanical stability (i.e. bubble collapse). The bubble collapse at R_{crit} is caused by an excessive pressure difference across the shell interface resulted from the gas outward diffusion.

The relation between $\overline{R_{crit}}$, which is defined as R_{crit} normalized by the initial particle radius (R), and the shell relevant parameters is provided in Eq. (5), where a more stable shell is found to exhibit a smaller $\overline{R_{crit}}$.

$$\Gamma\overline{R_{crit}}^5 + 3\overline{R_{crit}}^2\left(\overline{R_{crit}} - 1\right) + \frac{S}{R}\sqrt{\frac{(1+\upsilon) - \Gamma\overline{R_{crit}}^2}{3(1-\upsilon)}} = 0 \tag{5a}$$

with

$$\Gamma = \frac{\gamma_{sl} + \gamma_{sv}}{2G_S S}, \qquad \overline{R_{crit}} = \frac{R_{crit}}{R}, \qquad G_s = \frac{E}{2(1+\upsilon)} \tag{5b}$$

where γ_{sl} and γ_{sv} are the surface tensions at the solid–liquid and solid–vapour interfaces, respectively, υ is the Poisson's ratio, G_s is the shell rigidity modulus, and E is the Young's modulus.

In the present work, $\overline{R_{crit}}$ is used to quantify the shell mechanical stability of the hollow nanoparticulate aggregates. Following Krasovitski and Kimmel (2006), the values for γ_{sl} and γ_{sv} at the solid–water and solid–air interfaces are 0.04 and 0.005 N/m, respectively. The Young's modulus and Poisson's ratio values for solid PMMA reported in Ishiyama and Higo (2002) (i.e. $E \approx 3000$ MPa; $\upsilon = 0.35$) are employed to approximate the values for the PMMA-MeOPEGMA nanoparticulate aggregates.

3. Results and discussion

3.1. Impact of the spray drying parameters

The impacts of the spray drying parameters on the particle size, shape, and the shell thickness of the nanoparticulate aggregates are investigated using the 230 ± 80 nm PMMA-MeOPEGMA nanoparticles ($\rho_{true} = 1.3\ \mathrm{g/cm^3}$) at nanoparticle concentration of 0.8% (w/w). The spray drying parameters being examined are the feed rate and the drying gas flow rate, which govern the size and the evaporation rate of the spray droplet hence dictate the spray dried particle morphology. For this purpose, a full 2 × 2 factorial design is conducted in which the feed rate is varied between 1.4 and 4.2 mL/min, whereas the drying gas flow rate is varied between 240 and 350 L/h (Table 1). The inlet temperature is not varied and maintained at 110 °C as a higher inlet temperature leads to an outlet temperature that is higher than the glass transition temperature of the PMMA-MeOPEGMA causing the nanoparticles to deform and form a polymer film. On the other hand, a lower inlet temperature is

Table 1
The impact of spray drying parameters on the S/R ratio (230 ± 80 nm nanoparticles).

Run no.	Feed rate (mL/min)	Gas flow (L/h)	d_G (μm)	d_A (μm)	ρ_{eff}/ρ_{true}	S/R_{theory} (%)
A1	1.4	240	9.4 ± 3.9	4.6	0.18	7
A2	1.4	350	9.0 ± 3.5	3.5	0.12	4
A3	4.2	240	9.7 ± 4.4	3.5	0.10	3
A4	4.2	350	9.6 ± 4.6	3.9	0.13	4

insufficient to completely evaporate the water resulting in the formation of highly cohesive particles due to the excessive moisture content.

The SEM image of the spray dried particles in Fig. 2 indicates that the three types of particle morphology (i.e. types A, B, and C) are all present, which explains the wide particle size distribution presented in Table 1. Importantly, both the mean geometric (d_G) and aerodynamic (d_A) diameters of the spray dried particles in Table 1 are not greatly affected by the change in the spray drying parameters, where d_G remains to be equal to ≈9–10 μm and $d_A \approx 3$–4 μm. A t-test analysis using three independent measurements indicates that the changes in the d_G and d_A values as a function of the spray drying parameters are statistically insignificant.

Consequently, the theoretical S/R ratio, which is determined from the ratio of ρ_{eff}/ρ_{true} obtained using the mean d_G and d_A values, remains relatively constant at 3–4% for a majority of the runs. One exception is for the particles obtained at the lower limits of both the feed and the drying gas flow rates (Run no. A1), whose S/R ratio is slightly higher at 7% as a result of its larger d_A value. In the present work, the theoretical S/R ratio obtained from this method is experimentally validated using either SEM or TEM images. Examples of the validated particle samples are presented in the next section. Importantly, the very low S/R ratio indicates that the nanoparticulate aggregates are extremely hollow in which approximately 90% of the total particle volume is occupied by the gas. The calculated $\overline{R_{crit}}$ value of these particles is ≈95–96% signifying a weak mechanical stability, where a mere 4–5% reduction in the particle radius, as a result of the gas outward diffusion to the surrounding liquid, can create a pressure difference across the shell interface that is sufficient to completely destabilize the shell.

In summary, changing the spray drying parameters fails to produce hollow nanoparticulate aggregates with a wide range of S/R ratios, which is attributed to the insensitiveness of both the d_G and d_A values to the change in the spray drying condition. As a result, the S/R ratio is limited to a very narrow range (i.e. $3 \leq S/R \leq 7\%$) signifying a weak mechanical stability. Furthermore, the mean d_G of the hollow particles produced (≈9–10 μm) is equal to or larger than the blood capillary size, which would compromise their capillary passage hence jeopardize the applicability of the hollow nanoparticulate aggregates as an ultrasound contrast agent. Therefore, a formulation method to manufacture smaller size particles with a larger S/R ratio needs to be developed. The impact of changing the spray drying concentration of the nanoparticles is investigated for this purpose.

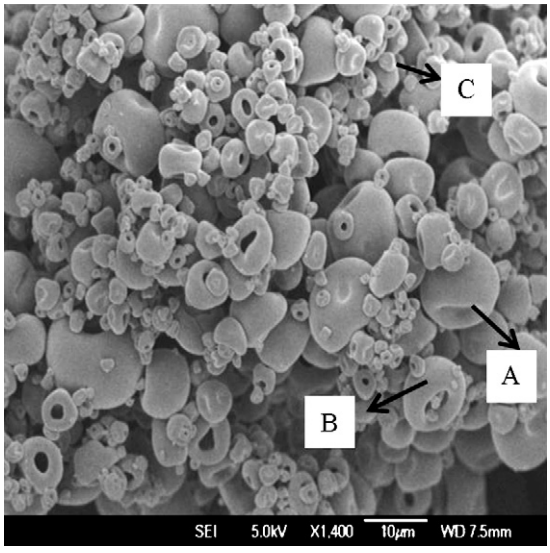

Fig. 2. SEM image of the hollow spherical nanoparticulate aggregates showing the three types of particle morphology (Run no. A1).

3.2. Impact of the nanoparticulate suspension concentration

The impacts of the spray drying concentration of the nanoparticles on the particle size, shape, and the shell thickness of the nanoparticulate aggregates are investigated again using the 230 ± 80 nm PMMA-MeOPEGMA nanoparticles. The nanoparticle concentration is varied between 0.5% and 2.5% (w/w) and the results are summarized in Table 2. The SEM image in Fig. 3a indicate that a majority of the spray dried particles are in the form of the dimpled spherical hollow aggregates and the very fine solid aggregates (i.e. types A and C morphology) having mean $d_G \approx 9$–10 μm with a wide particle size distribution (Table 2). A closer look at the dimpled sphere with a defected shell reveals its hollow structure.

A close-up view at the particle surface in Fig. 3b reveals that the shell constitutes of several layers of the nanoparticulate aggregates that form a gas-tight interface at the shell hence suited for use as an ultrasound contrast agent. The results in Table 2 indicate that both the mean geometric and aerodynamic diameters are not significantly affected by the change in the nanoparticle concentration. The mean d_G values only vary between 9 and 10 μm, whereas the mean d_A values remain constant at $d_A \approx 2.7$–2.8 μm for the range of nanoparticle concentration investigated. Again, a t-test analysis indicates that the changes in the mean d_G and d_A values as a function of the nanoparticle concentration is statistically insignificant.

The theoretical S/R ratio is calculated to be equal to 2–3%, which again signifies a weak mechanical stability of the shell ($\overline{R_{crit}} \approx 97\%$). To validate the theoretical S/R ratio, the shell thickness is measured from the SEM image in Fig. 3b and is found to be equal to ≈240 nm for particles with $d_G \approx 10$ μm, which translates to an S/R ratio of 5% that is comparable to the theoretical value of 2–3%. The procedure is repeated for particles of different d_G values from which it is concluded that the theoretical S/R ratio differs only by a few percentage points from the experimental value. Therefore, the S/R ratio characterization by the method described in Section 2.4 is proven to be reliable.

The investigation on the nanoparticle concentration effect is repeated using the 50 ± 20 nm PMMA-MeOPEGMA nanoparticles

Table 2
The impact of nanoparticulate suspension concentration on the S/R ratio (230 ± 80 nm nanoparticles).

Run no.	NP conc. (% w/w)	d_G (μm)	d_A (μm)	ρ_{eff}/ρ_{true}	S/R_{theory} (%)
B1	0.5	10.1 ± 4.3	2.7	0.05	2
B2	1.0	8.7 ± 4.0	2.8	0.08	3
B3	1.5	9.4 ± 4.3	2.8	0.07	2
B4	2.5	10.5 ± 4.5	2.8	0.05	2

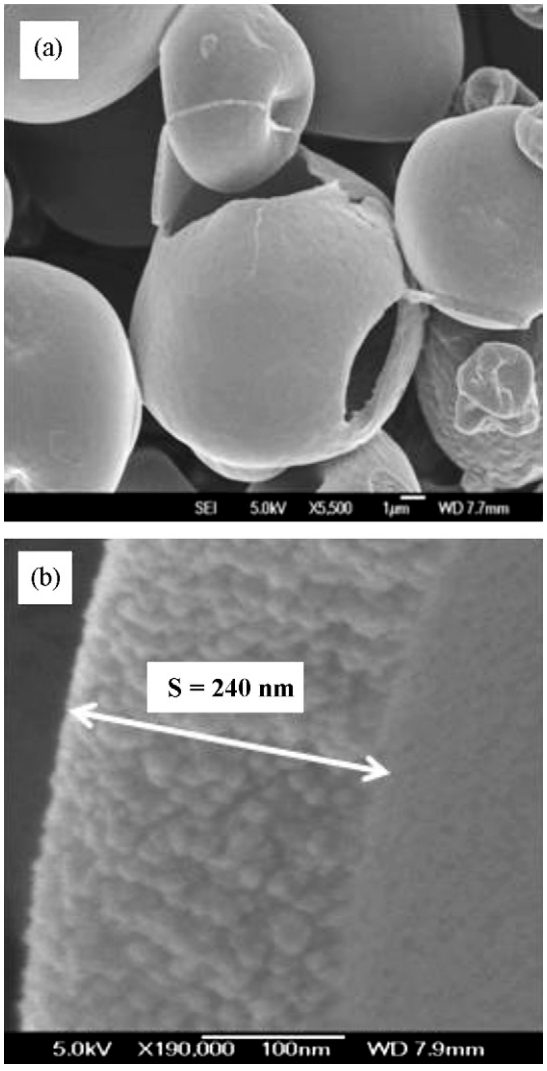

Fig. 3. SEM images of (a) hollow spherical nanoparticulate aggregates with mean $d_G \approx 9$–10 μm (Run no. B3) and (b) shell thickness validation.

in which the nanoparticle concentration is varied between 0.9% and 3.2% (w/w). The results in Table 3 again indicate that the S/R ratio is not significantly affected by the change in the nanoparticle concentration and the mean d_G value remains in the 8–10 μm range.

In summary, varying the nanoparticulate suspension concentration fails to produce hollow nanoparticulate aggregates with a wide range of S/R ratios for the two nanoparticle sizes investigated. This trend, which is similar to the result of varying the spray drying parameters, is caused by the inability of the current formulation method to produce hollow nanoparticulate aggregates of different mean d_G values (i.e. lower than 9–10 μm). For this reason, the impact of including a surfactant (i.e. phospholipids), which affects the spray droplet stability and consequently the droplet size, into the spray drying formulation is investigated.

Table 3
The impact of nanoparticulate suspension concentration on the S/R ratio (50 ± 20 nm nanoparticles).

Run no.	NP conc. (% w/w)	d_G (μm)	d_A (μm)	ρ_{eff}/ρ_{true}	S/R_{theory} (%)
C1	0.9	10.0 ± 3.8	3.0	0.07	2
C2	1.2	9.6 ± 3.4	2.5	0.05	2
C3	2.4	8.0 ± 3.3	3.1	0.12	4
C4	3.2	9.1 ± 3.7	2.6	0.06	2

3.3. Impact of the phospholipids inclusion

The inclusion of the phospholipids, which readily occupies the liquid–vapour interface of the evaporated droplet due to its surfactant nature, causes a competitive adsorption between the nanoparticles and the phospholipids molecules at the interface. As a result, a smaller area is available for the nanoparticles to aggregate affecting the shell formation process hence the resultant shell thickness. In addition, the presence of the phospholipids lowers the surface tension of the spray droplets, which reduces the droplet ability to maintain a large spherical shape throughout the drying process. Consequently, formation of smaller and less spherical nanoparticulate aggregates is anticipated to intensify with the phospholipids inclusion.

The impact of the nanoparticulate suspension concentration is re-examined in the presence of the phospholipids. The experiments are conducted using two nanoparticle sizes, 230 ± 80 and 110 ± 40 nm, at a constant phospholipids concentration of 0.2% (w/w). The results of the 230 ± 80 and 110 ± 40 nm nanoparticles are summarized in Tables 4 and 5, respectively. The results of the mean d_G values indicate that the spray dried particles of the 230 ± 80 nm nanoparticulate suspension exhibit a significantly smaller mean particle size ($d_G \approx 3$–6 μm) than that obtained using the 110 ± 40 nm nanoparticulate suspension ($d_G \approx 5$–10 μm). The results signify the dependence of the geometric size of the spray dried particles on the nanoparticle size, which is not evident in the absence of the phospholipids.

Importantly, the results of the 230 ± 80 nm nanoparticles indicate that nanoparticulate aggregates of lower d_G values can be obtained by including the phospholipids in the spray drying formulation. In contrast, the mean d_A values in Tables 4 and 5 remain relatively unaffected by the change in the nanoparticle concentration ($d_A \approx 3$ μm) despite the phospholipids inclusion. The lower d_G values are consistently observed for the 230 ± 80 nm nanoparticles in the range of the nanoparticle concentration investigated (Table 4), though the size reduction is diminished at nanoparticle concentrations above 1.5% (w/w). A similar size reduction, though to a lesser extent, is also observed for the 110 ± 40 nm nanoparticles data (Table 5) at nanoparticle concentrations above 1% (w/w).

Significantly, the plots of the particle size distribution in Fig. 4 indicate that including the phospholipids in the formulation (i.e. Runs No. D1 and E3) leads to a significantly more uniform particle size distribution with a lower mean d_G value compared to the formulation without the phospholipids (i.e. Run no. A1). The ability

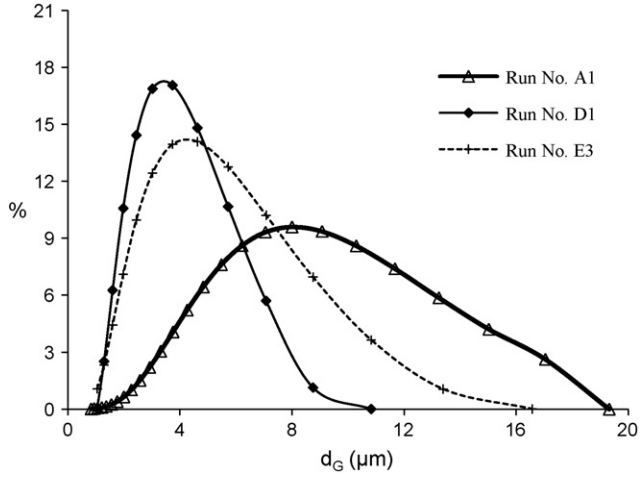

Fig. 4. Geometric particle size distributions of the different formulation methods.

Table 4
The impact of nanoparticulate suspension concentration on the S/R ratio in the presence of the phospholipids (230 ± 80 nm nanoparticles).

Run no.	NP conc. (% w/w)	Mean d_G (μm)	Median d_G (μm)	Mode d_G (μm)	d_A (μm)	ρ_{eff}/ρ_{true}	S/R_{theory} (%)
D1	0.5	4.3 ± 1.7	3.0	3.7	3.4	0.48	20
D2	1.0	3.1 ± 1.9	2.2	2.5	3.2	0.82	44
D3	1.5	3.4 ± 1.8	2.5	3.0	3.1	0.64	29
D4	2.5	5.9 ± 2.3	4.2	4.6	3.0	0.20	7

Table 5
The impact of nanoparticulate suspension concentration on the S/R ratio in the presence of the phospholipids (110 ± 40 nm nanoparticles).

Run no.	NP conc. (% w/w)	Mean d_G (μm)	Median d_G (μm)	Mode d_G (μm)	d_A (μm)	ρ_{eff}/ρ_{true}	S/R_{theory} (%)
E1	0.5	9.5 ± 5.0	5.6	5.7	3.7	0.12	4
E2	1.0	7.5 ± 4.0	4.1	4.6	2.7	0.10	3
E3	1.5	5.4 ± 2.7	3.2	3.7	3.2	0.27	10
E4	2.5	5.9 ± 2.8	3.7	4.6	2.9	0.19	7

of the current formulation method to produce a uniform particle size distribution is critical as the nanoparticulate aggregates are intended to be used as an ultrasound-mediated nanoparticulate drug delivery vehicle. Therefore, the ability to deliver a uniform therapeutic dose is essential.

The SEM image of the 230 ± 80 nm nanoparticulate aggregates in Fig. 5a at nanoparticle concentration of 0.5% (w/w) indicates that the spray dried particles maintain the dimpled spherical shape despite their significantly lower mean d_G values. A close-up view at the defected shell in Fig. 5b indicates that the hollow structure is preserved with an increased shell thickness in the range of several hundred nanometres. TEM images in Fig. 6 indicate that hollow nanoparticulate aggregates of Run no. D1 with $d_G \approx 6$ and 3 μm exhibit a shell thickness in the range of 1.5 and 0.5 μm, respectively, which translates to S/R ratios of approximately 50% and 30%, respectively. The mean theoretical S/R ratios of these particles in Table 4 are calculated to be equal to 20% hence the theoretical value is in the right order of magnitude with the experimental value.

At S/R ratio ≈20%, approximately 50% of the total particle volume is occupied by the gas compared to ≈90% at the lower S/R ratios of 2–4% obtained in the absence of the phospholipids. Importantly, the results in Table 4 indicate that the S/R ratio of the 230 ± 80 nm nanoparticulate aggregates can be further increased to ≈40% by increasing the nanoparticle concentration up to 1.0% (w/w) above which the S/R ratio starts to decrease back to 20%. The significant increase in the S/R ratio of the 230 ± 80 nm nanoparticulate aggregates, which is raised from below 10% to approximately 20–40% in the presence of the phospholipids, is caused by the hindered diffusive motion of the nanoparticles toward the liquid–vapour interface occupied by the phospholipids resulting in a larger shell thickness.

In contrast, the phospholipids inclusion does not lead to a significantly higher S/R ratio for the hollow aggregates of the 110 ± 40 nm nanoparticles (Table 5). The S/R ratios remain less than 10% for the range of the nanoparticle concentration investigated. This trend is attributed to the higher diffusivity of the 110 ± 40 nm nanoparticles compared to that of the 230 ± 80 nm attributed to their smaller particle size, such that the 110 ± 40 nm nanoparticles are less affected by the presence of the phospholipids at the interface.

Importantly, the higher S/R ratio of the 230 ± 80 nm nanoparticulate aggregates in the presence of the phospholipids results in a considerably lower $\overline{R_{crit}}$ value (≈80–90%). The lower $\overline{R_{crit}}$ value, which is shown in Fig. 7 to be inversely proportional to the S/R ratio, signifies a higher shell mechanical stability. The uniform mean particle size ($d_G \approx 3$–5 μm) and the high mechanical stability of the hollow particles obtained using the large nanoparticle size (230 ± 80 nm) with the phospholipids inclusion represent the two ideal features of an effective ultrasound contrast agent. Nevertheless, formulation involving smaller size nanoparticles is often needed in ultrasound-mediated nanoparticulate drug delivery to meet the therapeutic release requirement. For smaller size nanoparticles, such as the 110 ± 40 nm nanoparticles, the presence of the phospholipids at 0.2% (w/w) has been shown to be inadequate to produce hollow nanoparticulate aggregates having ideal mean particle size and shell mechanical stability.

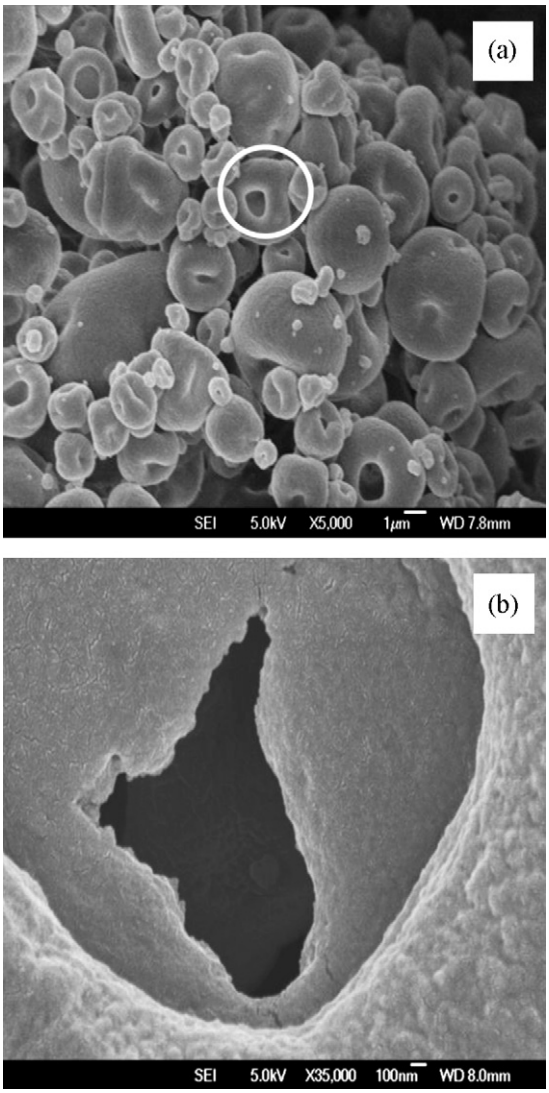

Fig. 5. SEM images of (a) dimpled spherical nanoparticulate aggregates with mean $d_G \approx 4$ μm and (b) the smaller size aggregates remain hollow (Run no. D1).

Table 6
The impact of phospholipids concentration on the S/R ratio (110 ± 40 nm nanoparticles).

Run no.	PL conc. (% w/w)	Mean d_G (μm)	Median d_G (μm)	Mode d_G (μm)	d_A (μm)	ρ_{eff}/ρ_{true}	S/R_{theory} (%)
F1	0.0	8.8 ± 4.5	5.1	5.7	4.1	0.17	6
F2	0.2	7.0 ± 3.5	4.5	5.7	3.2	0.16	6
F3	0.4	7.6 ± 3.9	4.6	5.7	4.7	0.29	11
F4	0.8	7.6 ± 3.5	4.7	5.7	4.5	0.27	10

For that reason, the impact of increasing the phospholipids concentration is examined at a constant nanoparticle concentration of 0.8% (w/w) using the 110 ± 40 nm nanoparticles. The results in Table 6 indicate that the mean d_G value of the hollow particles initially decreases with the phospholipids inclusion similar to the previous results. The S/R ratio of these smaller particles, however, is unaffected and remains low as the decrease in the mean d_G value is accompanied by a decrease in the d_A value. As the phospholipids concentration is increased from 0.2% to 0.8% (w/w), an opposite trend is observed, where both the mean d_G and d_A values increase proportionally resulting in relatively constant S/R ratios (≈6–11%). A further increase in the phospholipids concentration to 2% (w/w) leads to an increased formation of the crumpled solid aggregates (type C morphology) that are not suitable for use as an ultrasound contrast agent (Fig. 8).

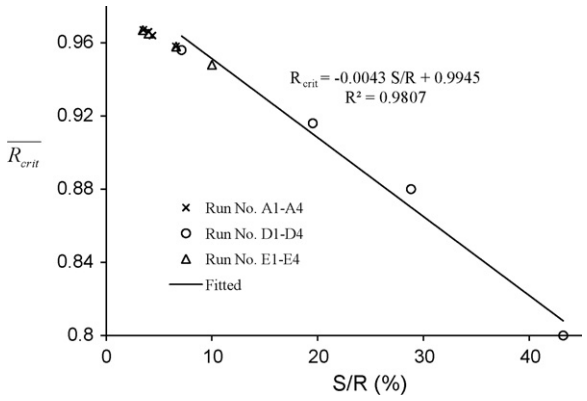

Fig. 7. Shell mechanical stability as a function of the S/R ratio.

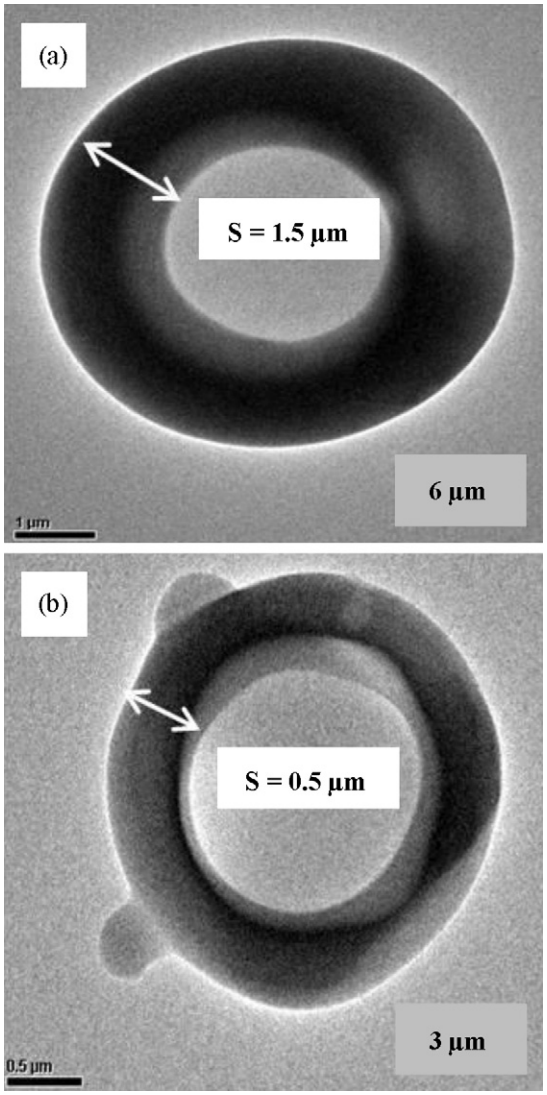

Fig. 6. TEM images of the hollow spherical nanoparticulate aggregates with d_G of (a) 6 μm and (b) 3 μm (Run no. D1).

In summary, the ability of the current formulation method to produce hollow nanoparticulate aggregates having the ideal mean particle size and shell mechanical stability is limited to the formulation involving large size nanoparticles (>200 μm) in the presence of the phospholipids. For smaller nanoparticle sizes, an investigation on the effects of the nanoparticulate suspension pH, which influences the colloidal stability of the nanoparticles hence their diffusivity, is being conducted and the results will be detailed in a forthcoming article. Nevertheless, the higher shell mechanical stability at higher S/R ratios is accompanied by a decrease in the total gas content of the hollow particles resulting in a lower echogenicity level of the ultrasound contrast agent. In other words, a trade-off exists between prolonging the lifespan of the ultrasound contrast agent and its echogenicity level.

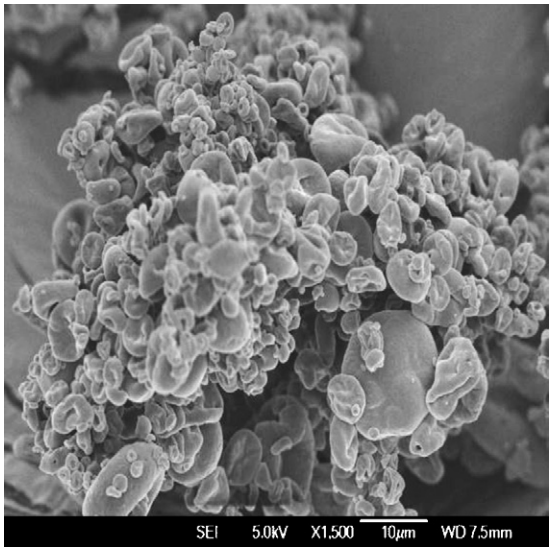

Fig. 8. SEM images of the nanoparticulate aggregates at 2% (w/w) phospholipids concentration.

4. Conclusion

A novel formulation technique to manufacture polymeric hollow spherical nanoparticulate aggregates with controllable shell thickness and particle size is developed for use as a potential ultrasound contrast agent. The principle mechanism is based on a spray drying technique in which a fast convective drying of nanoparticulate suspension droplets results in the formation of hollow spherical nanoparticulate aggregates. The impacts of different formulation variables on the shell mechanical stability of the hollow particles, which governs the effectiveness of the ultrasound contrast agent as well as its lifespan, are examined using a wide range of nanoparticle sizes. The results indicate that the shell mechanical stability of the hollow nanoparticulate aggregates is linearly dependent on the shell thickness-to-particle radius ratio (S/R ratio). In the absence of the phospholipids, varying the spray drying parameters and the nanoparticulate suspension concentration are found to have insignificant effects on the S/R ratio and the particle size. Without the phospholipids inclusion, large hollow nanoparticulate aggregates ($d_G \approx 10\,\mu m$) with a wide particle size distribution and a weak mechanical stability (i.e. low S/R ratio) are consistently produced at different nanoparticle concentrations and for different nanoparticle sizes. In contrast, formulations involving large size nanoparticles (>200 μm) in the presence of the phospholipids result in the formation of more uniform and smaller size hollow nanoparticulate aggregates ($d_G \approx 4\,\mu m$) with a significantly higher shell mechanical stability, which are ideal for use as an ultrasound contrast agent.

Acknowledgement

A financial support from Nanyang Technological University's Start-Up Grant (Grant No. SUG 8/07) is gratefully acknowledged.

Appendix A. Shell thickness to particle radius ratio

For a hollow sphere with a shell thickness S and a radius R, the ratio of S/R can be related to the true and effective particle densities by the following:

$$\rho_{eff} = \frac{m_{shell}}{V_{shell} + V_{core}}$$

$$\rho_{true} = \frac{m_{shell}}{V_{shell}}$$

$$\frac{\rho_{eff}}{\rho_{true}} = \frac{V_{shell}}{V_{shell} + V_{core}} = \frac{4/3\pi R^3 - 4/3\pi(R-S)^3}{4/3\pi R^3} = 1 - \left(\frac{R-S}{R}\right)^3$$

$$\frac{R-S}{R} = \left(1 - \frac{\rho_{eff}}{\rho_{true}}\right)^{1/3}$$

$$\frac{S}{R} = 1 - \left(1 - \frac{\rho_{eff}}{\rho_{true}}\right)^{1/3}$$

References

Bjerknes, K., Sontum, P.C., Smistad, G., Agerkvist, I., 1997. Preparation of polymeric microbubbles: formulation studies and product characterisation. Int. J. Pharm. 158, 129–136.
Chen, S.Y., et al., 2006. Efficient gene delivery to pancreatic islets with ultrasonic microbubble destruction technology. Proc. Natl. Acad. Sci. U.S.A. 103, 8469–8474.
Edwards, D.A., Dunbar, C., 2002. Bioengineering of therapeutic aerosols. Annu. Rev. Biomed. Eng. 4, 93–107.
El-Sherif, D.M., Wheatley, M.A., 2003. Development of a novel method for synthesis of a polymeric ultrasound contrast agent. J. Biomed. Mater. Res.: Part A 66A, 347–355.
Ferrara, K., Pollard, R., Borden, M., 2007. Ultrasound microbubble contrast agents: fundamentals and application to gene and drug delivery. Annu. Rev. Biomed. Eng. 9, 415–447.
Goertz, D.E., de Jong, N., van der Steen, A.F.W., 2007. Attenuation and size distribution measurements of definity (TM) and manipulated definity (TM) populations. Ultrasound Med. Biol. 33, 1376–1388.
Hadinoto, K., Zhu, K., Tan, R.B.H., 2007. Drug release study of large hollow nanoparticulate aggregates carrier particles for pulmonary delivery. Int. J. Pharm. 341, 195–206.
Ishiyama, C., Higo, Y., 2002. Effects of humidity on Young's modulus in poly(methyl methacrylate). J. Polym. Sci., Part B: Polym. Phys. 40, 460–465.
Krasovitski, B., Kimmel, E., 2006. Stability of an encapsulated bubble shell. Ultrasonics 44, 216–220.
Landau, L.D., Lifshitz, E.M., 1976. Mechanics, vol. 1. Pergamon Press, New York.
Lindner, J.R., 2004. Microbubbles in medical imaging: current applications and future directions. Nat. Rev. Drug Discovery 3, 527–532.
Lum, A.F.H., et al., 2006. Ultrasound radiation force enables targeted deposition of model drug carriers loaded on microbubbles. J. Controlled Release 111, 128–134.
Narayan, P., Wheatley, M.A., 1999. Preparation and characterization of hollow microcapsules for use as ultrasound contrast agents. Polym. Eng. Sci. 39, 2242–2255.
Pisani, E., et al., 2006. Polymeric nano/microcapsules of liquid perfluorocarbons for ultrasonic imaging: physical characterization. Langmuir 22, 4397–4402.
Raisinghani, A., DeMaria, A.N., 2001. Physical principles of microbubble ultrasound contrast agents. In: Symposium on Contrast Echocardiography (CE), Newport, Rhode Island, pp. 3J–7J.
Rossi, S., Waton, G., Krafft, M.P., 2008. Small phospholipid-coated gas bubbles can last longer than larger ones. Chemphyschem 9, 1982–1985.
Schmidt, W., Roessling, G., 2006. Novel manufacturing process of hollow polymer microspheres. Chem. Eng. Sci. 61, 4973–4981.
Straub, J.A., et al., 2005. Porous PLGA microparticles: AI-700, an intravenously administered ultrasound contrast agent for use in echocardiography. J. Controlled Release 108, 21–32.
Tsapis, N., et al., 2005. Onset of buckling in drying droplets of colloidal suspensions. Phys. Rev. Lett. 94.